Hindawi
Geofluids
Volume 2024, Article ID 4059478, 16 pages
https://doi.org/10.1155/2024/4059478

Research Article

Effect of Temperature Gradient on Compressive Strength and Strain Characteristics of Coarse-Grained Frozen Soil

Jiajun Luo,[1] Changtao Hu,[2,3] Zhilong Zhang,[1] Bingbing Lei,[2,3] Jing Luo,[1] Ao Zhang,[1] and Ge Hao[1]

[1]*College of Civil Engineering and Architecture, Xinjiang University, Urumqi 830049, China*
[2]*Xinjiang Transportation Planning Survey and Design Institute Co., Ltd., Urumqi, Xinjiang 830000, China*
[3]*Xinjiang Key Laboratory for Safety and Health of Transportation Infrastructure in Alpine and High Altitude Mountainous Areas, Urumqi, Xinjiang 830000, China*

Correspondence should be addressed to Zhilong Zhang; zhangzl@xju.edu.cn

Received 17 November 2023; Revised 20 February 2024; Accepted 22 February 2024; Published 13 March 2024

Academic Editor: Wensong Wang

The temperature field beneath a roadbed is asymmetrically distributed, which causes uneven settlement, longitudinal cracking, and even sliding and collapse, as well as other diseases of frozen soil roadbeds. Most roads in alpine mountain regions are half-filled and half-excavated. The degree and direction of the temperature gradient are utilized as variables in a numerical simulation to examine the deformation properties of coarse-grained frozen soil. The findings demonstrate that (1) coarse-grained frozen soil has a nonlinear connection between strength and the lowest temperature, with strength increasing with decreasing temperature and decreasing under the influence of the temperature gradient. (2) When an arbitrary temperature field acts on frozen soil, its monolithic character diminishes, its shear strength and maximum strength decrease as the angle θ increases, and the distribution of the shear zone takes the form of an X. (3) An asymmetrical shear zone forms when the direction of the temperature gradient θ deviates from 0°. The degree of asymmetry in the ground deformation and the angle of inclination of the shear zone are positively related to θ.

1. Introduction

The four phases of complex media referred to as frozen soil include solid earth, ice crystals, water, and air [1]. The characteristics of frozen soil and regular thawed soil differ significantly due to the presence of cemented ice in the former. Since frozen soil is a material with a multiphase composition, its nonuniformity is more noticeable. Additionally, because frozen soil is more closely related to regular soil composition due to the presence of more gel-coagulated ice, its nonuniformity is more significant [2, 3]. The mechanical properties of frozen soil will also change as its internal space changes. Numerous investigations on the strength properties of soils have been conducted worldwide [4–8]. In this research study, the primary objective is to understand the deformation characteristics of coarse-grained frozen soil as a function of temperature. Coarse-grained soil is a type of soil that is commonly found in nature, and according to foreign scholars, it generally has a particle size above 0.075 mm and a coarse-grain content of greater than 50% [9]. According to customary definitions, the coarse-grained soil industry in China is typically characterized as having a particle size greater than 0.075 mm or less than 60 mm of soil particles, and more than 50% of the soil must be coarse-grained with sand and gravel [10]. The temperature was employed as a variable by researchers [11, 12] to investigate how temperature affects the mechanical characteristics of coarse-grained frozen soil. Concurrently, numerous outstanding findings have come from related studies [13–15] that have examined the impact of compaction and moisture content in coarse-grained soils.

Frozen soil roadbed stability is primarily influenced by temperature and moisture content [16–18]. The strength of permafrost is impacted in high-altitude mountainous regions by the asymmetric shape of sloping permafrost roadbeds, which causes a tilt in the upper limit of permafrost and uneven temperature distribution. This nonuniformity makes the roadbed more prone to deformation, which could cause serious harm, and the associated frozen soil mechanic issues have not been well addressed [19–21]; therefore, research on the deformation characteristics of coarse-grained frozen soil under the action of an asymmetric temperature field has attracted increasing interest from researchers. The deformation of frozen soil is largely dependent on its mechanical characteristics. Several researchers have discovered via uniaxial compression tests that the strength of frozen soil increases linearly with temperature [22–27], while the elastic modulus of frozen sandy soil increases with increasing strain rate and decreasing temperature [28]. While the deformation of frozen walls calculated using nonuniform temperatures is relatively smaller than that calculated using the average temperature, in practical engineering, the temperature distribution of frozen soil is typically not uniform, and the nonuniform temperature field significantly affects the strength of artificially frozen walls [29, 30]. Another important factor influencing frozen soil strength is the temperature gradient [31]. At uniform temperatures, frozen soil strengthens significantly with decreasing temperature, but as temperature increases, frozen soil strength and strain approximately linearly decrease, with the temperature gradient-induced strength decay becoming more significant [32]. The distribution of cracks in frozen soil is also impacted by temperature gradients, which lead to stabilization, an increase, and a slow decrease in the crack area ratio [33]. Furthermore, the stress–strain and strength properties of frozen soil are influenced by the prefreeze moisture content, cooling temperature, and thawing temperature [34]. The damage morphology of frozen soil under various temperature gradients has also been demonstrated to exhibit distinct features. Furthermore, the temperature gradient has an impact on the destructive volumetric deformation and strength of frozen soil, causing the strength of frozen soil to diminish as the temperature gradient increases [35–37]. Consequently, the stability of frozen soil roadbeds depends critically on the temperature, temperature gradient, and mechanical characteristics.

The use of frozen soil in fine-scale investigations has been made possible by computer advancements [38, 39]. Additionally, a better understanding of the mechanical characteristics of soil bodies can be achieved by combining the macro- and micromechanical properties of geotechnical structures [40]. As a result, numerous related simulations have also been carried out by researchers in simulation studies of frozen soil numerical modeling. The relationship between microscopic coefficients and macroscopic parameters has been the subject of several studies [41, 42]. The changes in loess during the triaxial shear process were examined, and the changes in the soil particle displacement field and contact force field were found to be consistent with the macroscopic test results [43]. Based on these findings, it was determined that if the perimeter pressure in the simulation is not high enough, it may result in an increasingly extensive range of shear damage to the test material; conversely, as the perimeter pressure increases, the test material may experience ever-greater shear damage. A considerable linear damage range could result from an increase in the surrounding pressure [44, 45]. Triaxial tests of frozen soil under various peripheral pressures, temperatures, and strain rates are simulated indoors, and the cementation between soil and ice in frozen soil is simulated using the intrinsic model of discrete element software. In addition, using discrete element software, the viability of simulating frozen soil tests with discrete elements is verified, and the microdeformation mechanism and mechanical behavior of frozen soil are examined [46–48].

The majority of partially filled and excavated roads are utilized in alpine mountainous regions, which causes an uneven distribution of the temperature field and creates a step state where the temperature varies with soil depth. Researchers were interested in examining the impact of a temperature gradient on the original soil and the remodeled soil in the control test because of the establishment of a temperature gradient that alters the structural features of the soil [49]. Temperature gradients have been shown to have a diminishing effect on the strength and stiffness of frozen soil [50]. Investigators have examined the temperature gradient-induced frozen soil fracturing process and damage mechanism from an energy perspective in the study of nonhomogeneous evolution laws caused by temperature gradients [51, 52]. Numerical simulations of the effect of temperature gradients on the mechanical characteristics of frozen soils revealed that frozen walls are more vulnerable to damage from temperature gradients [53, 54].

In conclusion, despite various scholars dedicating their research efforts to investigating the impact of the temperature gradient on the strength characteristics of frozen soil, the available findings remain limited. Additionally, the use of discrete particle flow elements to simulate the distinctive structure of frozen soil and the adhesive properties of ice is still under exploration, resulting in a scarcity of studies in this area. Consequently, there is a dearth of information regarding the influence of the temperature gradient on the properties of frozen soil. Hence, this study focuses on coarse-grained frozen soil as the subject of investigation. Numerical simulation techniques were employed to construct a triaxial test numerical model, wherein the size and direction of the temperature gradient were considered variables. The objective was to examine the deformation characteristics of coarse-grained frozen soil subjected to an asymmetric temperature field.

2. Model

2.1. Type of Contact for the Model. The bonding of particles within frozen soil restricts deformation because of the ice content. The parallel bonding model is employed to replicate the adhesive impacts of ice on the soil particles that are present within frozen soil, hence leading to a more precise modeling of the movement of soil particles within frozen soil.

The parallel bonding model, depicted in Figure 1, posits that the bonding between ice particles and soil particles can

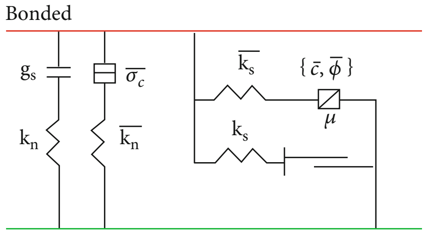

Figure 1: Schematic of the parallel bonding model (g_s: relative normal displacement; k_n: normal stiffness; $\overline{\sigma_c}$: tensile strength; $\overline{k_n}$: normal stiffness; $\overline{k_s}$: shear stiffness; $\bar{c}$: cohesion; $\bar{\Phi}$: friction angle; k_s: shear stiffness; μ: friction coefficient).

be likened to the formation of a bond within a specific range of contact points. This bond facilitates the transmission of contact forces and moments, resulting in shear strength in the normal direction and compressive strength in the tangential direction. Consequently, it imparts stiffness to the particles in both the normal and tangential directions. During the calculation process, the initial step involves determining the magnitude of stress exerted between the particles. If the stress surpasses the bonding strength, then the bonding becomes ineffective, resulting in the separation of the particles that were previously bonded together. Consequently, the bonds between the particles cease to exist, leaving only linear contact between the remaining portions of the particles.

2.2. Model Size and Particle Size. The optimal dimensions of a numerical sample and the quantity of particles within the sample are interconnected with the seamless functioning of the model. The insufficient size of the numerical specimen results in a limited number of generated particles within the specimen, compromising the model's integrity and the reliability of its conclusions. Conversely, selecting an excessively large numerical specimen with an excessive number of particles leads to an increased number of steps per iteration in the numerical computation, resulting in prolonged computation time and reduced computational efficiency. Hence, within the context of modeling, an approximate estimation of the quantity of particles present in a specimen can be obtained through the use of the following equation:

$$N = \left[\frac{L\pi R^2(1-n)}{\pi r^3}\right]. \quad (1)$$

In this context, the height of the specimen is denoted as L, while the width of the specimen and the average particle size of the frozen soil particles are standardized as R and r, respectively. Additionally, the initial porosity of the specimen is represented by the variable n, which is specified before creating the specimen.

According to the study, the particle gradation model of frozen soil exhibits a significant range of particle sizes, posing challenges for accurate calculations. However, when the ratio of the particle size to the characteristic length (L/R) is equal to or greater than 125, the particle size has a minimal impact on the various macroscopic parameters and simulation outcomes [55]. Therefore, in this research, the particle radius is increased by a factor of three to simplify the calculation process.

2.3. Fine-Scale Parameters for the Numerical Modeling of Three-Dimensional Particle Flows. In the particle flow model, the normal stiffness and tangential stiffness of the parallel bonding model, the normal stiffness and tangential stiffness of the linear contact part, and the parallel bond strength between them are the key parameters for determining the calculation results. Researchers have carried out a discrete elemental analysis on the bonding behavior of the frozen loess under different peripheral pressures and concluded that when the peripheral pressures were set at 0.5 MPa~2.0 MPa and the temperature was set to -6°C, the reasonable stiffness values range from 0.75×106 N/m~1.00×106 N/m, the normal bond strength is 232~900 N, and the friction coefficient is 0.50~1.85 [56]. The discrete meta-analysis of frozen sandy soil was carried out under different temperatures, and it was concluded that the particle contact stiffness was 6.2×106 N/m for a peripheral pressure of 0.2 MPa and a temperature of -10°C. A reasonable value for the particle contact stiffness was 6.2×106 N/m for a peripheral pressure from 0.5~2.0 MPa and a temperature of -6°C. A reasonable value for the particle contact stiffness was 6.2×10^7 N/m, the tangential bonding force was taken as 7000 N, a reasonable value for the normal bonding strength was 0.5×106 N/m~1×106 N/m, and a reasonable value for the friction coefficient is approximately 0.30 [57].

The current body of research indicates that temperature, water content, and strain rate are the primary determinants of the compressive strength of frozen soil [26, 58–60]. Only temperature and its angle of influence on frozen soil strength are considered in this paper to control the variables. Thermostatic triaxial investigations carried out by relevant researchers served as the basis for this work [61]. Using paramagnetic calibration, the abovementioned scholars ascertained the fundamental parameters of the specimens, which are displayed in Tables 1 and 2. Since every particle has the same beginning state in the discrete element calculations, the tangential and normal bonding strengths are also the same. Figure 2 shows the particle grading curves for the frozen soil samples.

2.4. Method of Determining the Size of the Temperature Gradient. The procedure for implementing temperature gradients of varying magnitudes in the model is as follows:

(1) In this paper, the repeated checks of current laboratory tests are fit [62, 63] because the particle bonding strength and the maximum bias stress are positively correlated. The maximum bias stress-temperature relationship curve is also drawn, the root distance is calculated from the maximum bias stress curve trend, and previous results from the literature [48] are incorporated into the two points at -5 and -2 degrees Celsius that correspond to the bond strength to derive $E(T)$. The change in the actual measured frozen soil strength is

Table 1: Numerical specimen model parameters.

Specimen size (mm)	Initial porosity ratio	Friction coefficient	Moisture content	Dry density ($g{\cdot}cm^{-3}$)	Percentage by volume	Frozen soil particle gradation (mm)
					50.00%	0.5~1
61.8*125	0.40	0.5	21.6%	1.76	33.33%	1~2
					16.67%	2~3

Table 2: Basic parameters of the numerical specimen.

Minimum particle size (mm)	Maximum particle size (mm)	Densities ($g{\cdot}cm^{-3}$)	Normal-to-shear stiffness ratio	Normal bond strength (kPa)	Tangential bond strength (kPa)	Wall friction coefficient
0.02	0.06	1.76	1	1.0×10^7	1.0×10^7	0.0

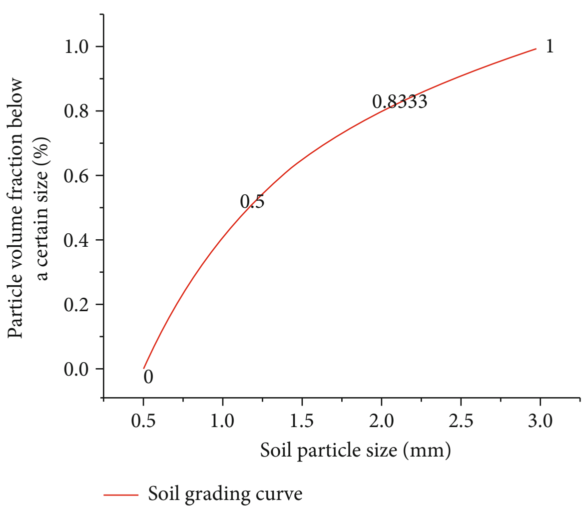

Figure 2: Frozen soil particle grading curves of model specimens.

consistent with the law of change [61]; the bond strength in the low-temperature region is large and decreases slightly with decreasing temperature. The curve reveals that in the high-temperature region, the bond strength is small, and the temperature decrease is large. In the low-temperature region, the bond strength is large, and as the temperature decreases, it decreases. Equation $E = (-2.52329 \cdot e^{T/2.18706} - 0.37644 \cdot e^{T/0.30567} + 3.64077) \cdot 10^{10}$, depicted in Figure 3, serves as the basis for this paper

(2) As illustrated in Figure 4, the temperature (T_a) of the particle exhibits a correlation with its position (Z_a). The relationship between $E(T)$ and $E(z)$ can be determined through the use of T_a and Z_a, considering the influence of varying temperature gradients

(3) The traversal structure in the FISH language is used in the Discrete Element 3D software "loop foreach cp contact.list("ball-ball")" to obtain a list of interparticle contacts ("ball-ball"). The Z-coordinate for particles in contact with tundra particles is traversed as follows: $i = \text{contact.id(cp)}$ and $z = \text{contact.pos.z(cp)}$. The corresponding bond strength E is obtained by evaluating the Z-coordinate. If contact.model(cp) = "linearpbond", then z_nianjiqiangdu $= E(Z)$. The cyclic contact flowchart is shown in Figure 5 (z_nianjiqiangdu: bond strength calibrated according to the vertical left z; $E(Z)$: bond strength values with respect to the vertical direction)

(4) In practical applications, the structure described in (3) can be successfully calculated. However, during the modeling process, it was found that when the model contains only 10,000 particles, it generates more than 30,000 interparticle contacts. Consequently, the structure needs to evaluate the Z-coordinate of each of the 10,000 particles, traverse the interparticle contacts, and assign values based on the Z-coordinate of the particles. This computational approach is both extensive and inefficient. Therefore, a simplified method is considered

(5) The goal of altering the bonding strength of the particles is accomplished by fitting the relationship between the vertical position of the particles and the bonding strength. This allows the temperature of the particles to change. To simplify the concept of calculus, the group of particles can be divided into smaller intervals (Z_a, Z_b) based on their Z coordinates. These intervals (Z_a, Z_b) correspond to different temperatures and represent distinct ball groups. By solving for the Z coordinate intervals of particles corresponding to each temperature gradient interval, the relationship between the temperature (T_a, T_b) and the bonding strength (E_a, E_b) can be transformed into a relationship between (Z_a, Z_b) and (E_a, E_b). The resulting value, E_{ab}, represents the bonding strength of the particles within the temperature interval. The process described simplifies the

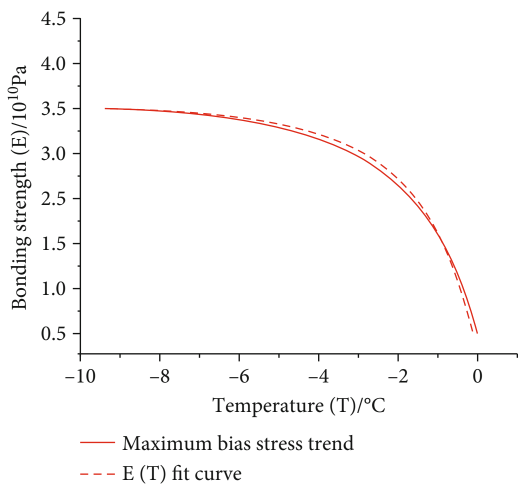

FIGURE 3: Temperature-bond strength functional relationship $E(T)$.

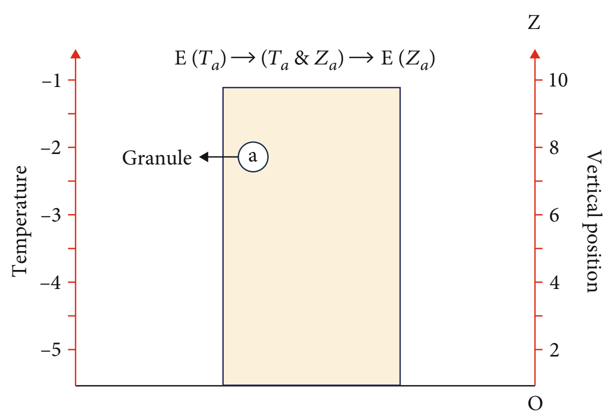

FIGURE 4: Schematic realization of the temperature gradient by the particle flow method.

procedure for determining the location of particles, leading to improved efficiency in assigning interparticle contact bond strength. Additionally, the effect is more satisfactory. In discrete element 3D, the method used to generate the model specimen is depicted in Figure 6(a). To demonstrate the effect of assigning different bond strengths to the layered model, Figure 6(b) is presented. To better illustrate the layered assignment of bond strength, contact behavior and instructions are utilized. It is necessary to employ contact behavior or instructions for calculating the bond between layers in the actual implementation

2.5. Method of Determining the Size of the Temperature Gradient. In accordance with the model incorporating a temperature gradient, each isothermal surface XoYT is consistently parallel to one another. Altering the inclination of the XoYT in relation to the XoY plane results in a modification of the temperature field direction. This enables the implementation of various magnitudes of temperature gradients on the model specimen. The functional structure is outlined as follows. The temperature gradient model is invoked using the restore command. Subsequently, 3DMAX software is utilized to construct a cylindrical geometry that closely matches the dimensions of the specimen. Within this geometry, horizontal disks are generated in a uniform manner, and these disks are positioned parallel to one another. The deflection angle of these disks in relation to the horizontal plane is adjusted to create a stratified geometry with varying tilt angles. The resulting geometry is then imported into Discrete Element 3D, where particles are organized based on the geometry and assigned corresponding parallel bond strengths. The resulting model, as depicted in Figure 7, is the final outcome of this process (XoYT: soil isothermal surface; XoY: level surface).

2.6. Conditions of the Assumption for Numerical Models in the Presence of an Asymmetric Temperature Field. To understand the role of the temperature gradient and asymmetric temperature field in the numerical simulation, the following assumptions must be made in this paper:

(1) In the vertical direction (Z), the temperature gradient is uniformly distributed and spaced, and the associated parallel bond strength is also fixed

(2) In real indoor triaxial compression tests, the distribution of nontemperature gradients within a sample changes as a result of heat exchange between the sample and the external environment after a temperature gradient environment is reached. The sample in this numerical simulation does not consider heat exchange and is able to constantly sustain this temperature gradient condition after allocating the parallel bonding strength between particles corresponding to the temperature gradient

(3) In real interior triaxial tests, the specimen's internal temperature distribution shifts when axial loading and confining pressure are applied. When confining pressure and axial loading are applied to the specimen in this numerical simulation, the temperature change caused by compression is disregarded, and the parallel bonding strength remains constant

(4) The lesser value of the parallel bonding strength in two-particle groups is chosen as the contact strength between frozen particles at different temperatures

(5) It is anticipated that the internal contact strength assignment of the original model will remain unchanged and will not be reallocated following the application of an asymmetric temperature field, regardless of the tilt angle of the temperature field

3. Effect of Temperature Gradient Magnitude on the Deformation of Coarse-Grained Permafrost

The temperature sensitivity of frozen soil is evident in its strength. As the temperature decreases, the ice content

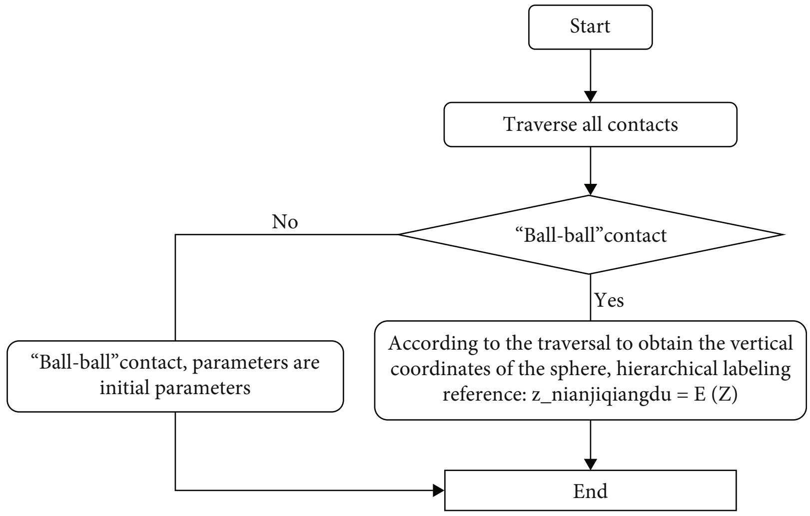

Figure 5: Loop and contact model flowchart.

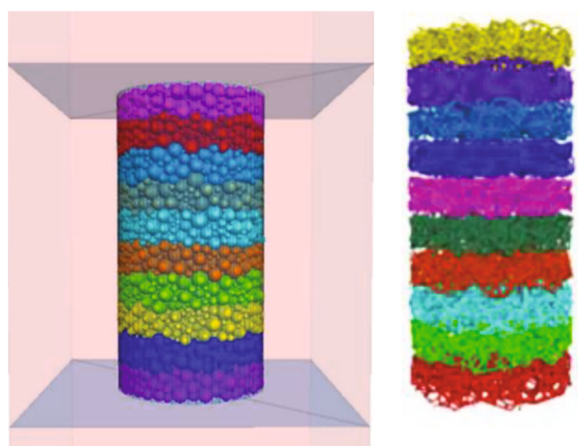

(a) (b)

Figure 6: Diagrammatic representation of the model used to achieve the temperature gradient condition: (a) schematic figure of the temperature gradient particles and (b) schematic representation of the model after parallel contact assignment.

within the frozen soil increases, leading to a stronger cementing action of ice on the soil particles. Consequently, the overall strength of the frozen soil is enhanced [34]. In this chapter, the temperature gradient in the numerical simulation is horizontally distributed and equally spaced. Four temperature gradient intervals, namely, 0~-8°C, 0~-3°C, 0~-5°C, and -5~-8°C, are chosen to conduct triaxial compression tests on the coarse-grained frozen soil numerical model. The test is performed under a peripheral pressure of 2.0 MPa and a strain rate of 1.25 mm/min. The objective is to investigate the impact of the temperature gradient on the strength of coarse-grained frozen soil while considering the influence of the peripheral pressure and strain rate. The findings of this study can serve as a valuable reference for future research in this field. This study is aimed at examining the impact of the temperature gradient on the strength of coarse-grained frozen soil. Additionally, the investigation considered the influence of the perimeter pressure and strain rate on the strength of coarse-grained frozen soil to establish a connection to the existing research in this field.

3.1. Stress–Strain Relationship of Coarse-Grained Frozen Soil under Different Temperature Gradients. Table 1 and Figure 2 display the sample particle size and the chosen coarse frozen soil particle size distribution. The strength of frozen soil is highly correlated with changes in bond strength in discrete element investigations, and there is little correlation with other parameters, according to [48]. Figure 3 shows the temperature–bond strength relationship, and the bond strength parameters corresponding to each temperature are plotted. Tables 3–6 display the parallel bond strengths chosen for each temperature gradient interval. The temperature of each numerical simulation specimen decreases gradually from top to bottom.

Figure 8 depicts the particle displacement under 15% strain at temperatures ranging from -5 to -8°C. The use of

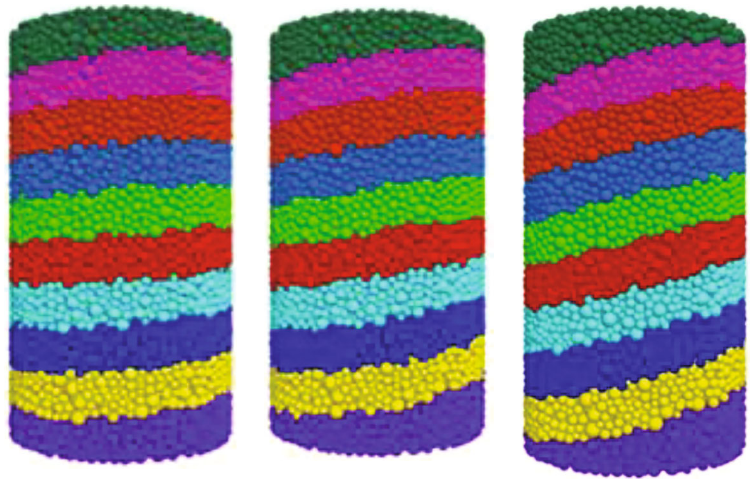

Figure 7: Diagrams showing how an asymmetric temperature field acts on model specimens: (a) 5° temperature tilt, (b) 10° temperature tilt, and (c) 15° temperature tilt.

Table 3: Parallel bond strength values for a temperature gradient of 0 to -8°C.

Pellet group temperature interval (°C)	Normal bond strength (Pa)	Tangential bond strength (Pa)	Vertical position interval (m)
0, -0.8	$14.4E+09$	$14.4E+09$	0.05, 0.0625
-0.8, -1.6	$21.8E+09$	$21.8E+09$	0.0375, 0.05
-1.6, -2.4	$26.3E+09$	$26.3E+09$	0.025, 0.0375
-2.4, -3.2	$29.4E+09$	$29.4E+09$	0.0125, 0.025
-3.2, -4	$31.5E+09$	$31.5E+09$	0, 0.0125
-4, -4.8	$33.0E+09$	$33.0E+09$	-0.0125, 0
-4.8, -5.6	$34.1E+09$	$34.1E+09$	-0.025, -0.0125
-5.6, -6.4	$34.8E+09$	$34.8E+09$	-0.0375, -0.025
-6.4, -7.2	$35.3E+09$	$35.3E+09$	-0.05, -0.0375
-7.2, -8	$35.6E+09$	$35.6E+09$	-0.0625, -0.05

Table 4: Parallel bond strength values for a temperature gradient of 0 to -5°C.

Pellet group temperature interval (°C)	Normal bond strength (Pa)	Tangential bond strength (Pa)	Vertical position interval (m)
0, -0.5	$12.2E+09$	$12.2E+09$	0.05, 0.0625
-0.5, -1.0	$18.2E+09$	$18.2E+09$	0.0375, 0.05
-1.0, -1.5	$22.1E+09$	$22.1E+09$	0.025, 0.0375
-1.5, -2.0	$25.1E+09$	$25.1E+09$	0.0125, 0.025
-2.0, -2.5	$27.4E+09$	$27.4E+09$	0, 0.0125
-2.5, -3.0	$29.2E+09$	$29.2E+09$	-0.0125, 0
-3.0, -3.5	$30.7E+09$	$30.7E+09$	-0.025, -0.0125
-3.5, -4.0	$31.9E+09$	$31.9E+09$	-0.0375, -0.025
-4.0, -4.5	$32.8E+09$	$32.8E+09$	-0.05, -0.0375
-4.5, -5.0	$33.5E+09$	$33.5E+09$	-0.0625, -0.05

Table 5: Parallel bond strength values for a temperature gradient of 0 to -3°C.

Pellet group temperature interval (°C)	Normal bond strength (Pa)	Tangential bond strength (Pa)	Vertical position interval (m)
0, -0.3	$10.5E + 09$	$10.5E + 09$	0.05, 0.0625
-0.3, -0.6	$15.0E + 09$	$15.0E + 09$	0.0375, 0.05
-0.6, -0.9	$18.2E + 09$	$18.2E + 09$	0.025, 0.0375
-0.9, -1.2	$20.7E + 09$	$20.7E + 09$	0.0125, 0.025
-1.2, -1.5	$22.8E + 09$	$22.8E + 09$	0, 0.0125
-1.5, -1.8	$24.5E + 09$	$24.5E + 09$	-0.0125, 0
-1.8, -2.1	$26.1E + 09$	$26.1E + 09$	-0.025, -0.0125
-2.1, -2.4	$27.4E + 09$	$27.4E + 09$	-0.0375, -0.025
-2.4, -2.7	$28.5E + 09$	$28.5E + 09$	-0.05, -0.0375
-2.7, -3.0	$29.6E + 09$	$29.6E + 09$	-0.0625, -0.05

Table 6: Parallel bond strength values for a temperature gradient of -5 to -8°C.

Pellet group temperature interval (°C)	Normal bond strength (Pa)	Tangential bond strength (Pa)	Vertical position interval (m)
-5.0, -5.3	$34.0E + 09$	$34.0E + 09$	0.05, 0.0625
-5.3, -5.6	$34.3E + 09$	$34.3E + 09$	0.0375, 0.05
-5.6, -5.9	$34.6E + 09$	$34.6E + 09$	0.025, 0.0375
-5.9, -6.2	$34.8E + 09$	$34.8E + 09$	0.0125, 0.025
-6.2, -6.5	$35.0E + 09$	$35.0E + 09$	0, 0.0125
-6.5, -6.8	$35.2E + 09$	$35.2E + 09$	-0.0125, 0
-6.8, -7.1	$35.4E + 09$	$35.4E + 09$	-0.025, -0.0125
-7.1, -7.4	$35.5E + 09$	$35.5E + 09$	-0.0375, -0.025
-7.4, -7.7	$35.6E + 09$	$35.6E + 09$	-0.05, -0.0375
-7.7, -8.0	$35.7E + 09$	$35.7E + 09$	-0.0625, -0.05

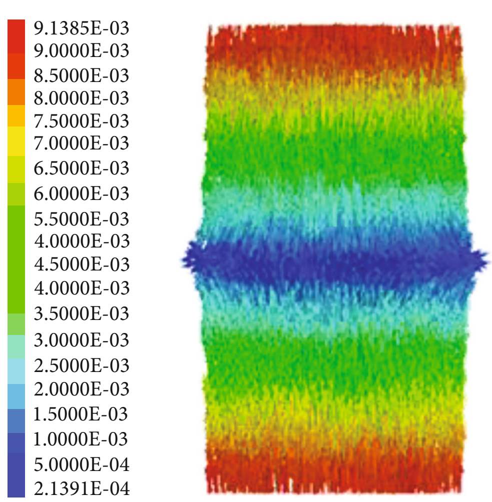

Figure 8: 15% strain state of frozen, coarse-grained soil at -5 to 8°C (unit: meters).

stiff walls in this simulation prevents intuitive observation of temperature gradients of 0-8°C, 0-5°C, 0-3°C, and -5-8°C. However, the particle numerical simulation movement chart clearly shows that the particles travel simultaneously from the middle and both sides. As a result, the temperature gradient is projected to have little effect on the compression deformation style of the sample.

By varying the magnitude of the temperature gradient, the stress–strain relationship obtained is as follows

Figure 9 illustrates the axial stress–strain relationship of frozen soil with coarse grains when subjected to varying temperature gradients. The strength of coarse-grained frozen soil is significantly affected by the temperature gradient. Additionally, in the temperature gradient intervals 0 ~-8°C, 0~-3°C, and 0~-5°C, in which the three highest temperatures all start from 0°C, the axial stress of the soil body increases gradually with decreasing temperature, and the corresponding peak strain increases, peaking at the temperature gradient of 0~-8°C, which is approximately 12.257 MPa. Meanwhile, compared with the experimental data for the constant temperature case by Yuan [48], it is observed that

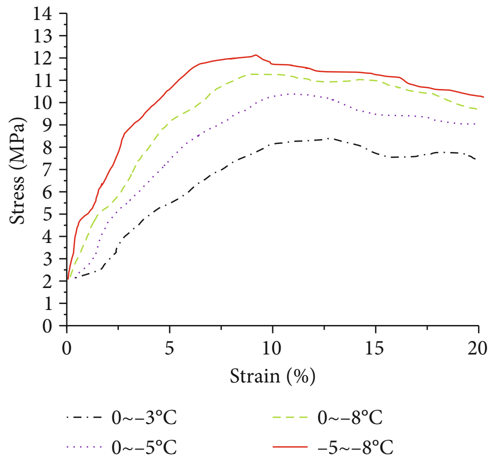

Figure 9: Coarse-grained frozen soil axial stress–strain relationship under various temperature gradients.

the peak axial stress of coarse-grained frozen soil under the action of a temperature gradient from 0 to -5°C is smaller than that in the case of constant temperature loading of -5°C. This is because the gluing effect of ice in the upper numerous temperature layers of frozen soil is weaker than the gluing effect at -5°C when the temperature gradient from 0 to -5°C is in effect. The value taken when defining the bond strength for these temperature layers will be smaller. The results obtained in this paper coincide with the fact that the strength of frozen soil under the effect of the temperature gradient in the macroscopic range will be smaller than that of frozen soil at a constant temperature. This demonstrates that it is valuable to consider the effect of the temperature gradient on the strength of coarse-grained frozen soil in this paper.

Table 7 illustrates how frozen soil particles react to temperature gradients. Along the direction of temperature decrease, the corresponding temperature layer is endowed with increased cohesive strength; the lower the minimum value of the selected temperature for the temperature gradient is, the greater the peak stress of the triaxial compression of coarse-grained frozen soil is, and the greater the strength of coarse-grained frozen soil is. When the temperature gradient is between -5 and 8°C, the frozen soil is in an overall low-temperature environment, and no new ice is formed by freezing. The strength of the frozen soil varies very little, which is most likely due to the different pore ice contents within the frozen soil in the actual low-temperature environment.

Furthermore, an analysis of the coarse-grained frozen soil curves at different temperature gradients shows that the stress–strain curves from the simulations at 0~5°C, 0~8°C, and -5~8°C are smoother when the frozen soil temperature decreases than those at 0~3°C. This phenomenon can be explained by the noticeable difference in the bonding effect of ice on frozen soil when the temperature gradient is between 0 and 3°C. The model illustrates this phenomenon by showing that there is a greater layer of particles in the high-temperature range in the frozen soil, in addition to a higher level of irregular movement between the particles. The percentage of permafrost in low-temperature environments increases, the bonding strength between layers varies less, the orientation trend of frozen soil particles after shear is evident, the force uniformity is enhanced, and the curves become smoother when the temperature decreases.

Table 7: Peak strength and corresponding strain of coarse-grained frozen soil under different temperature gradients.

Temperature gradient size (°C)	Peak intensity (MPa)	Strain (%)
0~-8	12.257	9.451
0~-5	11.675	10.656
0~-3	8.993	11.491
-5~-8	13.027	7.654

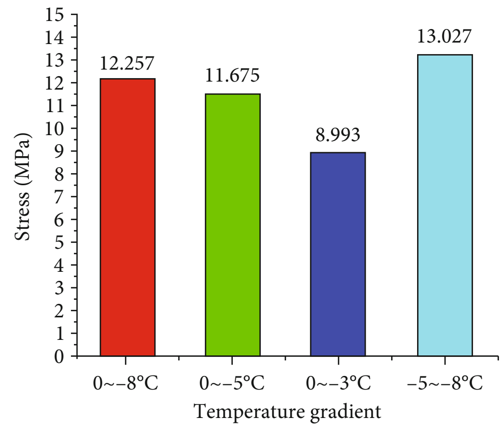

Figure 10: Effect of temperature gradient on the static properties of coarse-grained frozen soils.

Figure 9 shows the effect of the size of the temperature gradient on the static properties of coarse-grained frozen soil. As shown in Figure 10, the strength of coarse-grained frozen soil is enhanced when the minimum negative temperature of the temperature gradient is reduced, and the lower the minimum negative temperature of the temperature gradient is, the more obvious the effect of the strength enhancement of coarse-grained frozen soil is. When the temperature gradient starts at 0°C, which is the highest temperature, the peak strength of coarse-grained frozen soil increases with a decrease in the lowest negative temperature in the temperature gradient. Starting from 8.993 MPa at 0~-3°C to 11.675 MPa at 0~-5°C, the magnitude of the increase is approximately 29.8%, and from 11.675 MPa at 0~-5°C to 12.257 MPa at 0~-8°C, the magnitude of the increase is approximately 5.0%. This indicates that the process of the temperature gradient acting on coarse-grained frozen soil with the same maximum temperature is not linear. The minimum temperature decrease and the increase in the peak strength of frozen soil are not linear.

The numerical simulation results are consistent with the reality of frozen soil under the action of a temperature gradient; the ice content inside the layer at different temperatures varies, the temperature is higher inside the soil layer, the content of unfrozen water is high, the ice content is low, the strength of the soil body is lower because the influence of temperature is greater, and the temperature is lower in

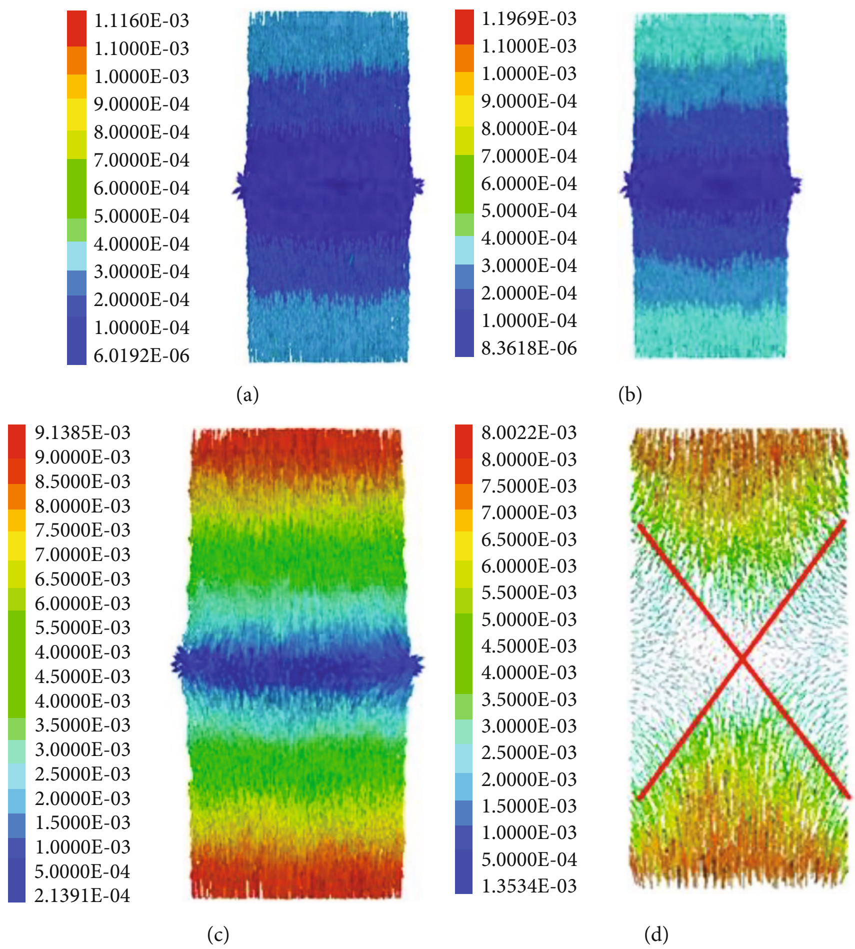

Figure 11: Particle displacements at different strains in coarse-grained frozen soil at 0~-8°C: (a) strain to 1%, (b) strain to 6%, (c) strain to 10%, and (d) strain to 18% (units: meters).

the soil layer. The magnitude of the increase is approximately 5.0%, indicating that when the temperature gradient acts on coarse-grained frozen soil, the process of decreasing the minimum temperature and increasing the peak strength of frozen soil is not linear when the maximum temperature is kept constant. The frozen soil strength is primarily determined by the ice inside the soil body; temperature has less of an impact. This means that the soil body's strength is greater in low-temperature environments than in high-temperature environments. The numerical simulation results also suggest that low-temperature environments are favorable for maintaining frozen soil stability.

3.2. Effect of the Temperature Gradient Magnitude on Shear Zones in Coarse-Grained Frozen Soil. The creation of a profile along the axis within the model enables the identification of particle movement in coarse-grained frozen soil under varying strains. Based on Zhou Jian's proposed theory on shear band formation [33], it is posited that the strain at which the specimen reaches its peak stress represents the primary moment when particle bonds are disrupted and the initiation of shear band formation occurs. Furthermore, the point in time after reaching peak stress that is characterized by strain signifies the stabilization of the shear band. This study focuses on the analysis of the development process of coarse-grained frozen soil shear zones under the influence of temperature gradients. Specifically, displacements at strains of 1%, 6%, 10%, and 18% are chosen for examination in this research.

Figure 11 shows the particle displacement at different strains of coarse-grained frozen soil from 0~-8°C. As shown in Figure 11(a), from 0~-8°C, when the strain is 1%, the coarse-grained frozen soil is at the beginning of loading, the particle displacement is mainly in the middle of the soil body in the middle of the position that appears to experience lateral displacement, and the adhesion between the particles is stronger. When the strain is 6%, the coarse-grained frozen soil experiences a period of loading, the lateral displacement of the particles in the middle of the soil body continues to increase, and the adhesion between particles is weakened, but adhesion is not destroyed. When the strain is 10%, the coarse-grained frozen soil reaches the peak stress, the intergranular bonding starts to break down, the displacement field starts to show a more pronounced inhomogeneous distribution, localized damage occurs, and shear zones start to form. When the strain is 18%, the coarse-grained frozen soil shear zone is fully formed. At this time, the shear zone is symmetrically X-shaped, the formation of this form of shear

Table 8: Coarse-grained frozen soil shear zone angle under the effect of different temperature gradient sizes.

Temperature gradient size (°C)	Shear band angle
0~-8	56.4°
0~-5	55.8°
0~-3	54.6°
-5~-8	57.1°

zone mainly shows that the model of the lateral stiffness is very large, as the lateral displacement of the soil body is very restrictive, and frozen soil cannot be stabilized in the same direction as the formation of the shear zone process takes place. Moreover, the angle is approximately 56.4°, which represents the angle of the formation of the shear zone, as depicted by the Moore-Cullen theory of classical geotechnics. The remainder of the temperature gradient of the shear band development process reveals that the development process is similar to a different temperature gradient size under the action of the frozen formation of coarse particles in terms of the angle of the shear band, as shown in Table 8. The temperature gradient size changes, and the formation of the angle of the shear band does not constitute a large difference. However, in terms of overall performance, to reduce the angle of the shear band and increase this phenomenon, the size of the temperature gradient is more consistent with that of the actual experimental measurements. Furthermore, the low-temperature environment of frozen soil strength is greater, and the stability of the characteristics is improved.

4. Relationship between the Direction of the Temperature Gradient and Deformation of Coarse-Grained Frozen Soil

Road construction in alpine mountainous regions is influenced by topographic limitations. To address these constraints, roadbeds that are partially filled and partially excavated are commonly employed. These roadbeds feature unidirectional slopes and exhibit distinct asymmetry in the distribution of temperature within the frozen soil layer. To assess the impact of this temperature asymmetry on the strength of coarse-grained frozen soil, numerical simulations are conducted to alter the direction of the temperature field. The objective is to simulate the effect of temperature field asymmetry and provide insights for real-world road projects.

4.1. Influence of the Direction of the Temperature Gradient on the Stress–Strain Relationship of Coarse-Grained Frozen Soil. The loaded coarse-grained frozen soil exhibits the following stress–strain relationship when the temperature gradient is oriented in a different direction.

Figures 12 and 13 and Table 9 illustrate the axial stress–strain relationship of coarse-grained frozen soil under various temperature gradients. Figure 12 illustrates the impact of the temperature gradient direction on the static properties of coarse-grained frozen soil. Table 9 illustrates the peak strengths and corresponding strains of coarse-grained frozen soil under various temperature gradients. The strength of

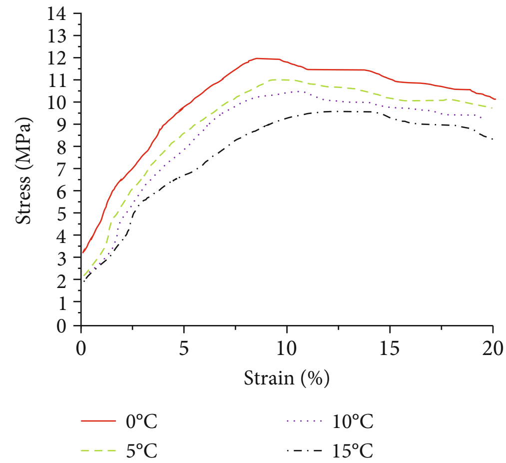

Figure 12: Axial stress–strain relationship of coarse-grained frozen soil under different directional temperature gradients.

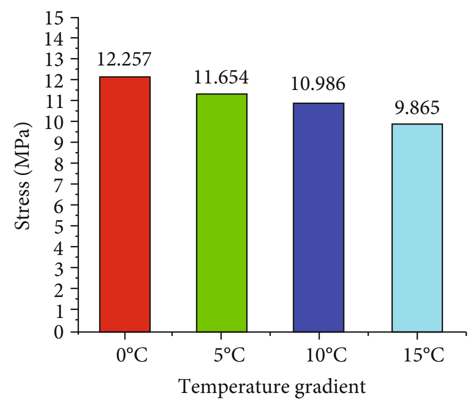

Figure 13: Influence of different temperature gradient inclinations on the static properties of coarse-grained frozen soils.

Table 9: Peak strength and corresponding strain of coarse-grained frozen soil in different temperature gradient directions.

Temperature gradient inclination (°)	Peak strength (MPa)	Strain (%)
0	12.257	9.451
5	11.654	10.187
10	10.986	11.423
15	9.865	12.260

coarse-grained frozen soils is impacted by the action of an asymmetric temperature field. For example, when the temperature gradient is inclined at an angle of 5°, the axial peak strength of coarse-grained frozen soil is 11.654 MPa, which is approximately 4.91% lower than the peak strength of 12.257 MPa when the temperature gradient is not inclined. Similarly, when the temperature gradient is inclined at an angle of 10°, the axial peak strength of the coarse-grained frozen soil is 10.986 MPa, which is a decrease of approximately 10.37%. The axial peak strength of coarse-grained frozen soil decreases by approximately 19.52% when the

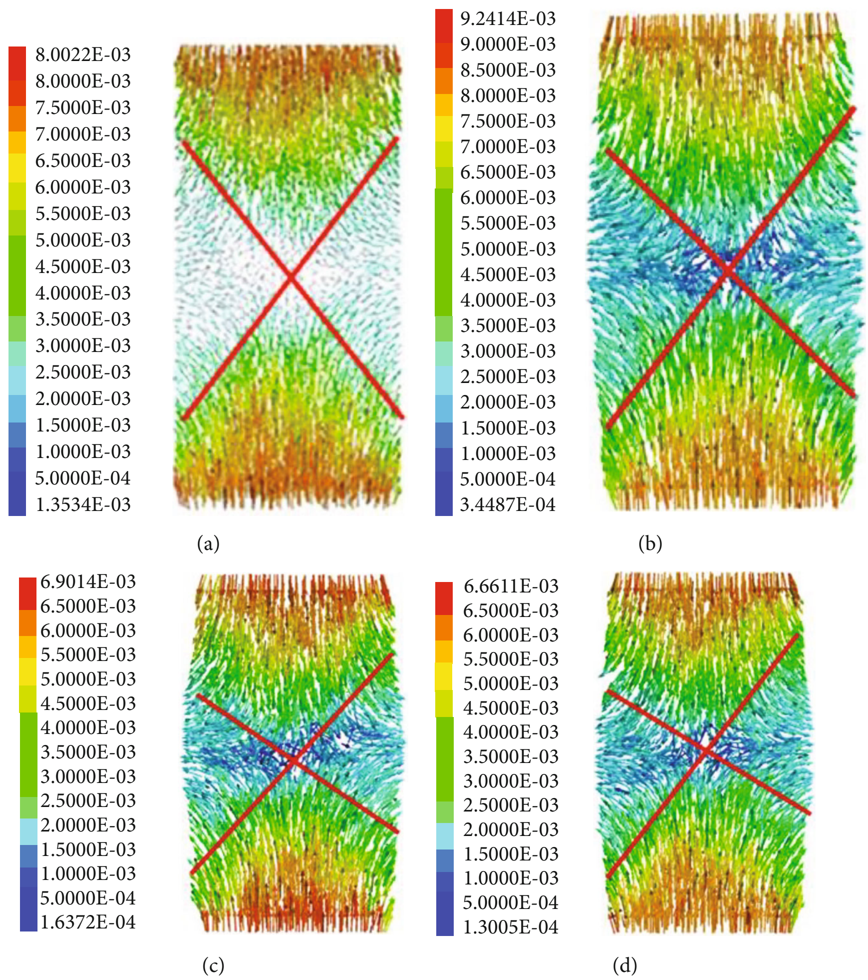

Figure 14: Displacement of coarse-grained frozen soil particles at various inclinations of the temperature gradient: (a) inclination of 0°, (b) inclination of 5°, (c) inclination of 10°, and (d) inclination of 15° (unit: meters).

temperature gradient inclination angle is 15°. This suggests that the strength of coarse-grained frozen soil decreases significantly as the temperature gradient inclination angle increases. Additionally, the strain corresponding to the peak strength decreases as the angle of the temperature gradient increases, which could be the cause of this result. After the occurrence of the inclination of the temperature gradient, the coarse particles of frozen soil in the compression process from the loading force F in terms of the isothermal surface perpendicular to the angle θ are decomposed into the same arrangement as the isothermal surface of the force $F \sin \theta$ that is perpendicular to the isothermal surface of the force $F \cos \theta$. The angle of inclination of the temperature gradient increases, the loading force F along the isothermal surface of the force $F \sin \theta$ increases, the bonding of the frozen soil particles by the shearing effect is strengthened, and this bonding is more prone to damage. Moreover, the bonding is more likely to be destroyed when tilth exists in frozen soil, and the bond strength between particles in each layer under the tilted grouping varies, weakening the structural integrity of the frozen soil. The stress–strain curve shows that the strain corresponding to the peak strength increases to 9.451% for a temperature gradient inclination angle from 0° to 12.260% for a temperature gradient angle of 15°. Therefore, it can be predicted that the strength of coarse-grained frozen soil will significantly decrease with increasing temperature field inclination under the action of the inclined temperature field. Furthermore, the coarse-grained frozen soil roadbeds in the alpine mountainous areas are prone to significant deformation in sloping sections, which affects road operation.

4.2. Characteristics of Shear Zones in Coarse-Grained Frozen Soil under the Action of the Temperature Gradient Direction. Based on the stress–strain relationship and the principles of soil mechanics, the strength of coarse-grained frozen soil is significantly influenced by the asymmetric temperature field resulting from different temperature gradient directions. Specifically, an increase in the temperature gradient leads to a decrease in frozen soil strength. Additionally, by examining the inclination angles of coarse-grained permafrost particles, it is possible to analyze the formation of shear zones and investigate the impact of the temperature field direction on the deformation of coarse-grained permafrost.

The coarse-grained frozen soil particle displacement is depicted in Figure 14 for temperature gradient inclination

Table 10: The angle of the portion of the shear zone with high temperature along the dip direction for different temperature gradient directions.

Temperature gradient size	Temperature gradient inclination	Shear band angle
0~-8°C	0°	56.4°
	5°	58.1°
	10°	59.4°
	15°	60.7°

angles of 0°, 5°, 10°, and 15° and temperature gradient sizes of 0~-8°C when the shear zone is fully developed. The X-type shear zones formed at temperature gradient inclination angles of 5°, 10°, and 15° are depicted in the figures. As expected, these shear zones are not symmetrically distributed like the X-type shear zones formed at 0°. Instead, they demonstrate that as the temperature gradient inclination angle increases, the degree of asymmetry in the distribution of the shear zones and the angle of the formed shear zones along the direction of the high-temperature portion of the temperature gradient inclination angle increase.

According to Table 10, the right half of the shear zone formed when the temperature gradient inclination angles are 5°, 10°, and 15° are approximately 58.1°, 59.4°, and 60.7°, respectively, and the increase in the number of degrees of the shear zone is not equal to the increase in the temperature gradient inclination. This is because each temperature layer is also tilted after the formation of the tilt angle of the temperature gradient, with the temperature of the frozen soil particles at the same horizontal position of the original temperature layer junction being different, which results in different parallel bond strengths and different interparticle bond sizes. The temperature layer junction becomes the weak surface of the overall coarse-grained frozen soil, the tilt angle increases, the bond between the layers is subjected to the strengthening of the shear effect, the time of the bond being destroyed is earlier than that in the horizontal distribution of the temperature gradient, and the time of the displacement of the same horizontal position of frozen soil particles is not synchronized. When the temperature gradient is horizontally distributed, the displacement time of frozen soil particles at the same horizontal position is not synchronized, resulting in the development of an asymmetric X-shaped shear zone on both sides. This simulation result indicates that the displacement of soil within the coarse-grained frozen soil road base is uneven under the influence of an asymmetric temperature field when subjected to external loads, leading to a greater likelihood of significant deformation.

5. Conclusions and Discussion

5.1. Conclusions. In this study, numerical analysis was employed to simulate the triaxial compression process of coarse-grained frozen soil under varying temperature gradients (in terms of both magnitude and direction). The findings are summarized as follows:

(1) In the process of modeling, the soil temperature gradients are represented by categorizing frozen soil particles based on their axial position relative to each isothermal layer of the temperature gradient. Subsequently, the fine-scale parameters associated with the temperature of each isothermal layer are assigned to the respective group of particles. This approach presents a novel perspective for investigating the deformation of frozen soil under the influence of an asymmetric temperature field

(2) The impact of changes in the temperature gradient size on the strength of coarse-grained frozen soil is readily apparent. In general, as the temperature gradient increases, the shear strength also increases. However, importantly, the relationship between the temperature gradient and peak strength is nonlinear. Specifically, when the temperature gradient is in the range of -5 to -8°C, the shear strength of frozen soil reaches its maximum value at 13.027 MPa. Additionally, it should be noted that different temperature gradient sizes result in the symmetric distribution of X-shaped shear zones within the loaded frozen soil formation

(3) The magnitude of the temperature gradient remains constant, while its direction varies with the axial angle θ of the soil samples. As a result, there is a notable decrease in the axial peak strength of frozen soil and an increase in the corresponding strain. Additionally, when the direction of the temperature gradient changes, the X-type shear zone that forms after frozen soil loading exhibits an asymmetric distribution. Specifically, at an axial angle of 15°, the inclination of the shear zone increases by 4.3°

5.2. Discussion. Although the results of numerical simulations have become increasingly close to real engineering situations as computers have advanced, there are still certain flaws and limitations in these simulations, and because of the restricted experimental conditions, they cannot be verified in practice.

(1) This article assumes that the temperature gradient is uniformly distributed vertically in the numerical simulation and that the related parallel bonding strength is fixed. In real studies, the temperature distribution state is more complex, and the sample is more likely to experience heat exchange with the surrounding outdoor air after sampling in accordance with the suggested temperature gradient circumstances. The sample's axial average distribution is not rigorously adhered to

(2) In real interior triaxial tests, the ice in a specimen melts, and the strength of the frozen soil changes when confining pressure and axial stress are applied. Nevertheless, this portion of the temperature shift was not replicated in the numerical simulation used for this paper when the specimen was subjected to

axial stress and confining pressure. Since it is believed that the temperature gradient does not change, the specified parallel bonding strength does not change. When comparing the obtained stress–strain relationship to the experimentally measured data, there can be some inaccuracies

Data Availability

The underlying data used to support the findings of this study are included within the article.

Disclosure

The design, implementation, data analysis, and writing of conclusions of this study were not influenced by any financial sponsor.

Conflicts of Interest

The authors declare that there are no conflicts of interest regarding the publication of this paper.

Authors' Contributions

J.L. was in charge of writing the original draft preparation. Z.Z. was responsible for the funding acquisition. J.L. was responsible for the visualization. A.Z. was responsible for the investigation. G.H. was responsible for the supervision. All authors have read and agreed to the published version of the manuscript. Jiajun Luo and Changtao Hu are co-first authors.

Acknowledgments

All the required funds were self-financed by the individual researcher or his affiliates.

References

[1] А. Цытович, *Frozen Soil Mechanics*, Science Press, 1985.

[2] P. A. Cundall and R. D. Hart, "Numerical Modeling of discontinua," *Analysis & Design Methods*, vol. 9, no. 2, pp. 231–243, 1993.

[3] Z. D. Cui, P. P. He, and W. H. Yang, "Mechanical properties of a silty clay subjected to freezing–thawing," *Cold Regions Science and Technology*, vol. 98, pp. 26–34, 2014.

[4] W. Wang, J. X. Zhong, and H. M. Wang, "Effect of polypropylene fiber on the unconfined compressive strength of loess with different water content," *Journal of Renewable Materials*, vol. 11, no. 4, pp. 1699–1714, 2023.

[5] H. Xing, L. Dongqing, M. Feng, B. Hui, and P. Wanwei, "Experimental study of the compressive and tensile strengths of artificial frozen soil," *Glaciology and Geocryology*, vol. 38, no. 5, pp. 1346–1352, 2016.

[6] W. Wensong, C. Guansen, L. Ye et al., "Experimental study of dynamic characteristics of tailings with different reconsolidation degrees after liquefaction," *Frontiers in Earth Science*, vol. 10, 2022.

[7] H. Jianyong, W. Jun, J. Dongfeng et al., "Construction technologies and mechanical effects of the pipe-jacking crossing anchor-cable group in soft stratum," *Frontiers in Earth Science*, vol. 10, 2023.

[8] L. Tianliang, Z. Wen, L. Run, H. Jianyong, J. Pengjiao, and C. Cheng, "Visualized direct shear test of the interface between gravelly sand and concrete pipe," *Canadian Geotechnical Journal*, vol. 61, no. 2, pp. 361–374, 2023.

[9] V. C. Xenaki and G. A. Athanasopoulos, "Liquefaction resistance of sand-silt mixtures: an experimental investigation of the effect of fines," *Soil Dynamics and Earthquake Engineering*, vol. 23, no. 3, pp. 1–12, 2003.

[10] R. F. Survey and Design Institute, "Geotechnical classification standard for railway engineering," China Railway Press, 2001.

[11] J. Bu and T. Wang, "Influences of freeze-thaw and fines content on mechanical properties of coarse-grained soil," *Chinese Journal of Geotechnical Engineering*, vol. 37, no. 4, pp. 608–614, 2015.

[12] W. Qingzhi, Z. Xinxin, L. Jiankun, L. Peng, and L. Zhenya, "Experimental study on direct shear tests of coarse-grained fillings of high-speed railway subgrade in cold region," *Journal of the China Railway Society*, vol. 38, no. 8, pp. 102–109, 2016.

[13] Z. Li and P. Li, "The variety regulation of gravel soil shear strength index during the direct shear test," *Technique of Seepage Control*, vol. 8, no. 1, pp. 11–14, 2002.

[14] W. Houzhen, W. Nim, H. Mingjian, and X. Xueyong, "Strength behaviour of gravelly soil with different water content in Jiangjiagou Ravine," *Journal of Soil and Water Conservation*, vol. 22, no. 5, pp. 221–224, 2008.

[15] W. Song, Z. Jungao, Q. Qihu, and L. Fan, "Particle breakage of coarse-grained materials in triaxial tests," *Chinese Journal of Geotechnical Engineering*, vol. 31, no. 4, pp. 533–538, 2009.

[16] W. Ma and D. Wang, *Frozen Soil Mechanics*, Science Press, 2014.

[17] Y. Lai, M. Liao, and K. Hu, "A constitutive model of frozen saline sandy soil based on energy dissipation theory," *International Journal of Plasticity*, vol. 78, pp. 84–113, 2016.

[18] X. Xu, Q. Li, Y. Lai, W. Pang, and R. Zhang, "Effect of moisture content on mechanical and damage behavior of frozen loess under triaxial condition along with different confining pressures," *Cold Regions Science and Technology*, vol. 157, 2019.

[19] J. M. Ting, R. T. Martin, and C. C. Ladd, "echanisms of strength for frozen sand," *Journal of Geotechnical Engineering*, vol. 109, no. 10, pp. 1286–1302, 1983.

[20] T. Wang and M. Dou, "Analysis on transverse thermal difference of embankment in frozen soil region," *Coal Geology & Exploration*, vol. 1, pp. 45–47, 2004.

[21] W. Xiaojun, H. Wenfeng, J. Fuqiang et al., "Dissection and analysis of settlement of rubble ventilation embankment and crack of ordinary embankment in frozen soil regions," *Journal of Rock Mechanics and Geotechnical Engineering*, vol. 25, no. 9, pp. 1904–1911, 2006.

[22] W. Fu, N. Wang, M. G. Hu, and Y. H. Xiang, "Study of relationship between uniaxial compressive strength and electrical resistivity of frozen soil under different temperatures," *Rock and Soil Mechanics*, vol. 30, no. 1, pp. 73–78, 2009.

[23] F. H. Sayles and D. L. Carbee, "Strength of frozen silt as a function of ice content and dry unit weight," *Engineering Geology*, vol. 18, no. 1–4, pp. 55–66, 1981.

[24] F. D. K. Haynes and A. Jack, *Effect of Temperature on the Strength of Frozen Silt*, Department of Defense, Department of the Army, Corps of Engineers, Cold Regions Research and Engineering Laboratory, 1977.

[25] Y. Q. Ma, "Tensile strength, uniaxial compressive strength test on artificially frozen soils," *Rock and Soil Mechanics*, vol. 17, no. 3, pp. 76–81, 1996.

[26] J. Zhang, H. Li, C. Lin, and Y. Zhu, "Compressive strength of saturated frozen silt under constant strain rate," *Chinese Journal of Rock Mechanics and Engineering*, vol. 22, no. 2, pp. 2865–2870, 2003.

[27] X. Haibin, "Relationship between uniaxial compressive strength of artificially frozen soil and temperature and moisture content," *Geotechnical Engineering World*, vol. 4, pp. 62–76, 2008.

[28] R. A. Bragg and O. B. Andersland, "Strain rate, temperature, and sample size effects on compression and tensile properties of frozen sand," *Developments in Geotechnical Engineering*, vol. 28, pp. 35–46, 1982.

[29] Z.-W. Wu, W. Ma, C.-Q. Zhang, and Z.-Y. Shen, "Strength characteristics of frozen sandy soil," *Journal of Glaciology and Geocryology*, vol. 16, no. 1, pp. 15–20, 1994.

[30] R. J. Chen, G. D. Cheng, S. X. Li, X. M. Guo, and L. N. Zhu, "Development and prospect of research on application of artificial ground freezing," *Chinese Journal of Geotechnical Engineering*, vol. 22, no. 1, pp. 43–47, 2000.

[31] G. S. Yang and J. Zhang, "Finite element numerical simulation of deep foundation pit excavation supported by frozen soil wall with nonhomogeneous temperature distribution," vol. 22, Tech. Rep. 2, Chinese Journal of Rock Mechanics and Engineering, 2003.

[32] G. Shao, "Investigation on testing apparatus for frozen soils with radial thermal gradient and deformation failure characteristics of frozen hollow cylinder under uniaxial compression, [M.S. thesis]," China University of Mining and Technology, Xuzhou, China, 2014.

[33] W. Jiao, "Experimental study on deformation and fracture of ice-rich frozen soils in thermal gradient environment, [M.S. thesis]," China University of Mining and Technology, Xuzhou, China, 2019.

[34] J. K. Liu and L. Y. Peng, "Experimental study on the unconfined compression of a thawing soil," *Cold Regions Science & Technology*, vol. 58, no. 1–2, pp. 92–96, 2009.

[35] X. Zhao, G. Zhou, and S. Li, "Research on deviatoric stress variation laws for deep frozen clay at different temperature gradients," *Chinese Journal of Rock Mechanics and Engineering*, vol. 28, pp. 1646–1651, 2009.

[36] X. Zhao, G. Zhou, and G. Chen Zhou, "Failure modes and compression strength of frozen clay under thermal gradient," *Chinese Journal of Geotechnical Engineering*, vol. 32, no. 12, pp. 1854–1860, 2010.

[37] Y. G. Yang, "Studies on the strength and constitutive models of frozen slit, [Ph.D. thesis]," Graduate School of Chinese Academy of Sciences, Hefei, China, 2011.

[38] C. J. Coetzee and D. N. Els, "Calibration of granular material parameters for DEM modelling and numerical verification by blade-granular material interaction," *Optics Communications*, vol. 46, no. 1, pp. 15–26, 2009.

[39] T. H. Tran, R. Venier, and B. Cambou, "Discrete modelling of rock-ageing in rockfill dams," *Computers and Geotechnics*, vol. 36, no. 1–2, pp. 264–275, 2009.

[40] Xie, "Reflections on soil mechanics in the 21st century," *Chinese Journal of Geotechnical Engineering*, vol. 4, pp. 111–114, 1997.

[41] B. Zhou, H. B. Wang, W. F. Zhao, J. W. Li, and B. C. Zheng, "Analysis of relationship between particle mesoscopic and macroscopic mechanical parameters of cohesive materials," *Journal of Rock Mechanics and Geotechnical Engineering*, vol. 33, no. 10, pp. 3171–3178, 2012.

[42] S. M. Xu, D. S. Ling, Y. M. Chen, and B. Huang, "Correlation of microscopic and macroscopic elastic constants of granular materials based on linear contact model," *Chinese Journal of Geotechnical Engineering*, vol. 32, pp. 991–998, 2010.

[43] S. Li, C. Wang, J. Ma, and G. Wang, "Microscopic changes of Longxi loess during triaxial shear process," *Journal of Rock Mechanics and Geotechnical Engineering*, vol. 34, pp. 3299–3305, 2013.

[44] J. Zhou and Y. Ji, "Mesomechanical simulation of sand mechanical properties," *Rock and Soil Mechanics*, vol. 24, no. 6, pp. 901–906, 2003.

[45] J. Zhou, X. Liao, Y. Ji, and J. Xu, "Simulating plane strain test of soils by particle flow code," *Journal of Tongji University (Natural Science)*, vol. 30, no. 9, pp. 1044–1050, 2002.

[46] F. Zhou and Y. Lai, "Simulation of mechanical behavior for frozen sand clay by discrete element method," *Rock and Soil Mechanics*, vol. 31, pp. 4016–4020, 2010.

[47] N. Yin, S. Li, W. Pei, M. Zhang, and Y. Dong, "Microscopic deformation mechanisms of triaxial test of frozen clay analyzed by discrete element method," *Journal of Glaciology and Geocryology*, vol. 38, no. 1, pp. 178–185, 2016.

[48] W. Yuan, "Triaxial compressive strength and deformation mechanism of frozen sand, [Ph.D. thesis]," Lanzhou University, Lanzhou, China, 2020.

[49] G. Lu, "Experimental study on mechanical properties for warm frozen soils in frozen soil regions, [Ph.D. thesis]," China University of Mining and Technology, Xuzhou, China, 2015.

[50] G. Q. Zhou, X. D. Zhao, and S. Li, "Stress-strain properties for the frozen media sand at different temperature gradients during two stress paths," *Chinese Journal of Geotechnical Engineering*, vol. 32, no. 3, pp. 338–343, 2010.

[51] X. Zhao, G. Zhou, and S. Li, "Deformation properties of frozen sand during loading and unloading in the presence of a thermal gradient," *Journal of China University of Mining & Technology*, vol. 39, no. 2, pp. 158–162, 2010.

[52] X. D. Zhao and G. Q. Zhou, "Creep deformation and heterogeneous characteristics for frozen soils with thermal gradient," *Chinese Journal of Geotechnical Engineering*, vol. 36, no. 2, pp. 390–394, 2014.

[53] J. Wang, *Research on the mechanical properties of inhomogeneous thick frozen wall in deep alluvium*, China University of Mining and Technology, Xuzhou, China, 2008.

[54] L. Hiting, *Research on the mechanical properties of inhomogeneous frozen wall with water-abundant bed rock*, Xi'an University of Science and Technology, Xi'an, China, 2013.

[55] S. Hui, W. Dong, B. Hu, and C. Qu, *Application of Discrete Element Particle Flow in Hydraulic and Geotechnical Engineering*, Science Press, 2017.

[56] N. Yin, S. Li, Y. Shi, Z. Sun, and Z. Yin, "Discrete element analysis of cemented behavior of frozen loess under different confining pressures," *Journal of Glaciology and Geocryology*, vol. 39, pp. 858–867, 2017.

[57] L. An, "Macro- and meso-mechanical properties of frozen soil and meso-deformation mechanism of subgrade, [Ph.D. thesis]," Harbin Institute of Technology, Haerbin, China, 2018.

[58] Y. Zhu, "Studies on strength ang creep behaviour of frozen soils in China," *Journal of Glaciology and Geocryology*, vol. 10, no. 3, pp. 332–337, 1988.

[59] L. Haipeng, L. Chuannian, Z. Junbing, and Z. Yuanlin, "Uniaxial compressive strength of saturated frozen clay at constant strain rate," *Chinese Journal of Geotechnical Engineering*, vol. 26, no. 1, pp. 105–109, 2004.

[60] S. Li, L. Gao, and S. Chai, "Significance and interaction of factors on mechanical properties of frozen soil," *Rock and Soil Mechanics*, vol. 33, no. 4, pp. 1173–1177, 2012.

[61] X. Z. Xu, *Frozen Soil Physics*, Science Press, 2010.

[62] L. Ma, Q. Jilin, F. Yu, and Y. Xiaoliang, "Experimental study on variability in mechanical properties of a frozen sand as determined in triaxial compression tests," *Acta Geotechnica*, vol. 11, no. 1, pp. 61–70, 2016.

[63] Y. Zhang, "Study on the influence of loading and unloading rate on the mechanical properties of frozen sand under true triaxial stress," 2022.